JOURNAL OF APPLIED CRYSTALLOGRAPHY
ISSN 1600-5767

Resolving pseudosymmetry in γ-TiAl using cross-correlation electron backscatter diffraction with dynamically simulated reference patterns

Brian Jackson,[a] David Fullwood,[a]* Jordan Christensen[a] and Stuart Wright[b]

[a]Mechanical Engineering Department, Brigham Young University, Provo, UT 84602, USA, and [b]EDAX/TSL, Draper, UT, USA. *Correspondence e-mail: dfullwood@byu.edu

Received 20 June 2017
Accepted 5 March 2018

Edited by A. Barty, DESY, Hamburg, Germany

Keywords: simulated cross-correlation electron backscatter diffraction; CC-EBSD; high-resolution electron backscatter diffraction; HR-EBSD; pseudosymmetry; titanium aluminides.

Pseudosymmetry is a phenomenon that occurs when grains with different lattice parameters produce nearly identical diffraction patterns such that conventional electron backscatter diffraction (EBSD) techniques are unable to unambiguously differentiate the lattice orientations. This commonly occurs in materials with near-unity tetragonality, such as γ-TiAl. The current study uses cross-correlation EBSD to resolve pseudosymmetry in γ-TiAl. Three dynamically simulated reference patterns are generated for each point in the scan, one for each of the three potential pseudosymmetric orientations, which are subsequently correlated with the original pattern using six different methods in order to identify the correct orientation. The methods are first applied to a scan of dynamically simulated patterns, which is used to evaluate the sensitivity of the method to pattern resolution, pattern noise and pattern center error. It was determined that all six methods were 100% successful up to about 13 µm of pattern center error and pattern resolutions of about 80 × 80 pixels, and hence the methods were applied to an experimental sample of lamellar γ-TiAl. A hybrid combination of two of the methods was shown to successfully select the correct pseudosymmetry for about 96% of the points in the scan, improving upon the 70% accuracy of the Hough-based methods for the current study and 90% accuracy for previous studies resolving pseudosymmetry in lamellar γ-TiAl.

1. Introduction

Electron backscatter diffraction (EBSD) is a common method of analyzing the microstructure of materials composed of crystalline lattices. By bombarding a material sample with an electron beam, diffracted electrons that exit the sample surface are intercepted by a screen. The resulting electron backscatter diffraction pattern (EBSP), captured using a low-light camera, can be analyzed to obtain information about the crystal structure and orientation. By scanning areas of the sample and collecting EBSPs at multiple locations, the orientation information obtained from EBSP analysis can be used to identify grains in polycrystalline materials, analyze grain boundary characteristics and perform texture analysis (Adams *et al.*, 1993; Schwartz *et al.*, 2009). Traditional EBSP analysis techniques utilize Hough transforms to identify band positions. The Hough transform maps a line in an image to an intercept and angle on a scatter plot; EBSD bands are transformed to 'Hough peaks' in Hough space, which are then used to determine the orientation of the crystal on the basis of a specified lattice structure; this process is often referred to as 'indexing'. Automated methods for indexing EBSPs are commonly used, generally *via* software that directly controls the scanning electron microscope used to collect the patterns. The precision of the orientation determination is typically

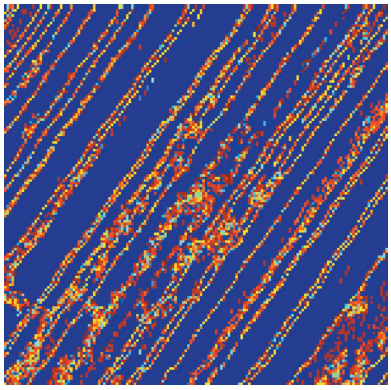

some fraction of a degree (Wright *et al.*, 2012, 2014; Ram *et al.*, 2015).

Currently, automated Hough-based indexing algorithms have difficulty resolving pseudosymmetry (Zambaldi *et al.*, 2009; Nolze *et al.*, 2016; Dey, Morawiec *et al.*, 2006; Dey, Bouzy & Hazotte, 2006; Simkin *et al.*, 2003; Sankaran *et al.*, 2009). Pseudosymmetry occurs when two patterns have nearly identical band positioning but unique crystallographic orientations, as shown in Fig. 1; to the naked eye, the patterns appear identical, but they have subtle differences that need to be resolved. Pseudosymmetry is commonly found in materials with a near-cubic lattice structure where one of the three principal axes is slightly longer than the other two. Tetragonality is the measurement of relative elongation of the longer axis and is defined according to the following formula (Vaudin *et al.*, 2015):

$$\varepsilon^{\text{tet}} = c - (a + b)/2, \tag{1}$$

where a, b and c are the lattice constants.

Titanium aluminides (commonly used in commercial aero-engines), martensite (an extremely hard phase of steel) and lead zirconate titanate are common engineering materials with a tetragonal lattice structure that exhibit pseudosymmetry. In γ-TiAl, for instance, the ratio c/a is usually about 1.02. Resolution of pseudosymmetric orientations in these materials is important in identifying the slip systems that uniquely contribute to their strength and hardening characteristics.

Several approaches have been used to resolve pseudosymmetry. Zambaldi *et al.* (2009) proposed using a fit characteristic of the indexing algorithm – or the angular deviation between the measured and expected Hough peak vectors – to correctly identify orientations in pseudosymmetric materials. This approach achieved a successful indexing rate up to 90% in a sample of lamellar γ-TiAl. Other recent approaches have used high-resolution, or cross-correlation, EBSD techniques to attempt to resolve pseudosymmetry (Nolze *et al.*, 2016; Oxford Instruments NanoAnalysis, 2016).

High-resolution EBSD (HR-EBSD), or cross correlation EBSD (CC-EBSD), extends the precision of traditional Hough methods by correlating deformations of the pattern with deformations of the lattice in all three dimensions. The shifts required to align the two regions are calculated using the convolution of many sub-regions of the patterns through the use of fast Fourier transforms. The combined effects of these shifts are then used to calculate the relative distortion and disorientation between the two patterns. This technique offers excellent relative orientation determination, several orders of magnitude better than Hough techniques (Troost *et al.*, 1993; Wilkinson *et al.*, 2006; Kacher *et al.*, 2009). Although CC-EBSD is typically applied to the measurement of strain between patterns, the current paper will be applying the same technique to detect subtle differences between pseudosymmetric patterns. Essentially, even when two strain-free patterns match closely but not perfectly, the deformation between them and their 'pseudostrain' will be small, whereas patterns that do not match will have a larger relative deformation and 'pseudostrain'. The ability of CC-EBSD to capture and quantify minute differences between patterns is the basis for its application to resolving pseudosymmetries.

Within the CC-EBSD technique there are two fundamental approaches for selecting the reference pattern: selecting an experimental pattern or generating a simulated pattern. The traditional method selects a pattern from the same grain as the pattern of interest, typically from a centralized location in the grain that is expected to have the lowest distortion (Wilkinson *et al.*, 2006). One reason for the more extensive use of experimental, or 'real', reference patterns (as opposed to simulated reference patterns) is the difficulty of accurately determining microscope geometry for replication in the simulated patterns (Britton & Wilkinson, 2012; Alkorta, 2013). Since a real reference pattern comes from the same microscope arrangement, the typical uncertainty in microscope geometry can be tolerated in the determination of relative distortion. However, because the absolute orientation of the reference pattern is not necessarily known, the ability to resolve pseudosymmetric patterns is limited.

The second reference pattern approach consists of generating a simulated reference pattern. Since the distortion and orientation of the simulated pattern are precisely known, the relative distortion and orientation information generated by the cross-correlation approach can theoretically determine the absolute distortion and orientation of the experimental

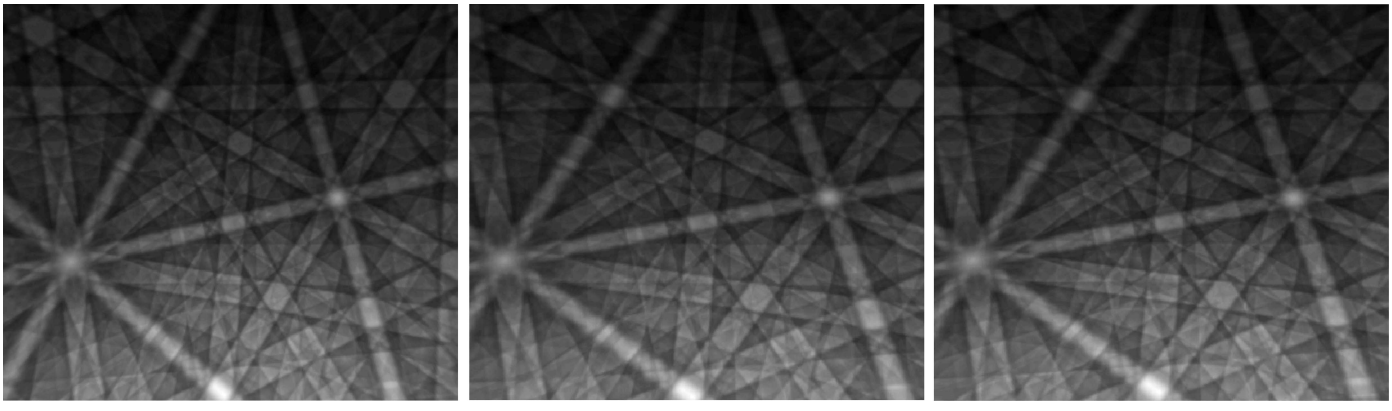

Figure 1
Simulated EBSPs of three pseudosymmetric lattices of γ-TiAl.

pattern. The determination of absolute distortion allows for the calculation of absolute strain and therefore tetragonality, which can be used to resolve pseudosymmetric orientations *via* identification of the elongated tetragonal axis, or *c* axis.

Furthermore, if a quantitative measure of tetragonality is not required, several methods exist within HR-EBSD to calculate a quantitative measure of fit, or correlation, between the experimental pattern and reference patterns that reflect different pseudosymmetric options. Although pseudosymmetric orientations have nearly identical band positions, their band intensity profiles – composed of band intensities and band widths – are unique, such that they can often be resolved by visual inspection of magnified images (Zambaldi *et al.*, 2009). Hence, a pixel-by-pixel comparison of the correlation between the experimental and reference images may adequately resolve pseudosymmetry (Nolze *et al.*, 2016).

There are currently two principal methodologies used to generate simulated EBSPs: kinematical simulation and dynamical simulation. Kinematical simulations are simplistic simulations based on Bragg's law; this approach defines positions for which constructive interference of scattered electrons occurs, from lattice planes of a specified interplanar spacing. Kinematical simulations accurately replicate band positions, but they suffer from poor band profile and intensity replication, especially near band axes. However, because of the simplistic nature of the simulation, they can be generated very quickly using efficient algorithms, typically in under a second (Kacher *et al.*, 2009, 2010; Fullwood *et al.*, 2015). Dynamical simulations, on the other hand, are based on a Monte Carlo simulation which computes the trajectories of individual electrons as they interact with the crystal and undergo scattering events (Callahan & De Graef, 2013; Minkelmann *et al.*, 2007). By simulating the trajectories of several million electrons, a high-fidelity EBSP can be generated that accurately replicates band position, profile and intensity (Winkelmann, 2010). The Monte Carlo simulation is extremely computationally intensive, taking anywhere from 6 to 30 min, depending upon the type of graphics card available (Jackson *et al.*, 2016), or hours for lower-symmetry materials; however, once the initial 'master' EBSD pattern is generated by the Monte Carlo simulation, patterns for individual orientations of the material can be quickly generated (<1 s). Since accurate simulation of band profiles is likely to be very important in resolving pseudosymmetry, and dynamically simulated patterns have been shown to be both more accurate and more precise than kinematically simulated patterns at low levels of relative strain between the experimental and reference patterns (Jackson *et al.*, 2016), dynamically simulated patterns were considered the better option for resolving pseudosymmetry in this study.

As briefly discussed above, accurate determination of microscope geometry presents a significant challenge when using simulated reference patterns. The pattern center of an EBSP, defined as the location where the electrons impinge normal to the surface of the detector screen, can have a significant effect on the calculation of absolute strain and tetragonality. If the assumed pattern center is incorrect, the reference pattern will be slightly shifted relative to the experimental pattern, resulting in artificial differences between the two patterns. Since pseudosymmetric orientations so closely resemble each other, it is imperative that the pattern center error is small; otherwise an incorrect orientation may be selected as the correct one. The sensitivity of the above methodologies to pattern center error is analyzed, and methods for minimizing the influence of pattern center error on resolution of pseudosymmetry are assessed.

It is also desirable to know how sensitive the methodology is to poor pattern quality. Several factors can affect pattern quality, including poor sample polish, internal structural entropy, electronic and detector noise, and low electron yield. Current methods for resolving pseudosymmetry, such as superlattice reflection detection using EBSD with long exposure times and high acceleration voltages or transmission electron microscopy analysis, are dependent upon extremely careful sample preparation and laborious or time-insensitive measurement processes (Zambaldi *et al.*, 2009; Dey, Morawiec *et al.*, 2006). Therefore, if the current methodology is able to work with sub-optimal patterns, it will have an advantage over other more exacting methods.

In summary, the purpose of the current paper is to expand upon previous studies investigating the effectiveness of using cross-correlation EBSD with dynamically simulated reference patterns to discern subtle differences between pseudosymmetric orientations in order to correctly identify the lattice orientation. Several potential methods for discerning these differences, including both CC-EBSD techniques and holistic pattern comparison techniques, will be used in an attempt to resolve pseudosymmetry in a common engineering material. Additionally, the effects of pattern center error, pattern resolution and pattern quality on the accuracy of this resolution will be evaluated.

2. Methods

2.1. Material samples

The current study used γ-TiAl to evaluate the effectiveness of HR-EBSD with a dynamically simulated reference pattern in resolving pseudosymmetry. Owing to its low density, nearly constant yield strength up to 1073 K, and good corrosion and creep resistance, γ-TiAl is an excellent choice of material in high-temperature structural components, such as in jet engines and turbines. The structure of the γ-TiAl phase is a face-centered-cubic derived tetragonal lattice. The *c* axis is about 2% longer than the *a* axis as a result of the alternating layers of titanium and aluminium that occupy the (002) planes. This results in three pseudosymmetric orientations, all separated by successive 120° rotations about the (111) plane normal. A detailed description of orientation variants and the domain structure of γ-TiAl is given by Zambaldi *et al.* (2009).

The ability to resolve pseudosymmetry, and thus better characterize the detailed microstructure, will aid the understanding of deformation modes and related strength and hardening characteristics in this important engineering

Table 1
Lattice parameters for γ-TiAl used by *EMsoft* and *OpenXY*.

Parameter	Value
a	0.4003 nm
b	0.4003 nm
c	0.4067 nm
Space group	123
Debye–Waller	0.006 nm^2

material. Additionally, γ-TiAl was selected as an appropriate material for this study given the existing literature dealing with γ-TiAl and its pseudosymmetric variants (Dey, Morawiec *et al.*, 2006; Zambaldi *et al.*, 2009; Dey, Bouzy & Hazotte, 2006; Sankaran *et al.*, 2009; Nolze *et al.*, 2016; Simkin *et al.*, 2003).

Both a simulated and an experimental scan of EBSPs were created as testbeds for the different pseudosymmetry resolution methods. In the case of the simulated scan, the pseudosymmetry is exactly known. For each method, dynamically simulated patterns were correlated with the test scan EBSPs to determine the correct lattice orientation, and the methods were compared in terms of their effectiveness.

2.1.1. Simulated scan. The first step in determining the effectiveness of the proposed methodology involved generating a simulated scan of γ-TiAl. Since the orientation, lattice parameters and microscope geometry can be exactly specified using simulated patterns, a controlled experiment investigating the ability of dynamically simulated reference patterns to resolve pseudosymmetry could be performed without having to account for variables such as sample preparation, pattern quality, pattern center error and uncertainty in lattice parameters.

The simulated patterns were generated by *EMsoft 3.0*, an open-source software package for simulation of electron diffraction and imaging modalities developed at Carnegie Mellon University (De Graef, 2015). As a precursor to generating patterns, a 'master' EBSD pattern was formed *via* the Monte Carlo approach, using the material parameters listed in Table 1, 20 keV accelerating voltage, 70° sample tilt and a resolution of 1024 × 1024 pixels. All other parameters were set to their default values.

After generating the 'master' EBSD pattern, from which any arbitrary orientation can be generated, a series of patterns were created in order to simulate an actual EBSD scan. This simulated scan was designed to consist of ten grains composed of ten patterns each. The orientation within each grain varied by 1° over the ten points within the grain (therefore a 0.1° misorientation between neighboring points of the same grain). This was done so that 100 unique orientations were generated, while having easily identifiable sections in the scan. Since pseudosymmetric orientations for γ-TiAl come in trios, three grains were all set to be pseudosymmetric to each other. With ten grains, three sets of pseudosymmetric grains were generated, while the last remaining grain was assigned a random orientation. The orientations were arranged such that one set of pseudosymmetric grains has all three grains adjacent, the other set has two adjacent grains and the third has all three grains separated. The adjacency of pseudosymmetric grains was chosen to test the dependence of a given pseudosymmetry algorithm accuracy on different transitions between pseudosymmetric orientations. The pattern center was adjusted for each point to match the simulated positions of the scan points. The sample tilt and azimuth, camera tilt and azimuth, accelerating voltage, and phosphor screen size were kept at their default values. The scan was replicated along three rows so that the indexing software could process the scan.

2.1.2. Experimental scan. A sample of γ-TiAl with a composition of 50% Ti and 50% Al with a lamellar microstructure was prepared by first grinding using 320 grit SiC paper, then polishing with a 9 µm polycrystalline diamond polish, and finally polishing with 0.05 µm colloidal silica. After sample preparation the EBSD patterns were collected using an FEI Helios Nanolab 600 scanning electron microscope with an accelerating voltage of 30 keV, a sample tilt of 70° and a camera elevation of 10°. A 150 × 151 point scan was taken with a step size of 0.2 µm, resulting in a scan area of about 30 × 30 µm.

2.2. Sample analysis

Once the scan was generated, it was indexed using the *OIM Data Collection 7.2* software developed by EDAX-TSL (EDAX, 2015). All of the points in the scan were identified as γ-TiAl: no hexagonal Ti_3Al was identified. It was expected that the indexing would not be able to resolve all of the orientations. The results of the indexing were then analyzed in *OpenXY*, an open-source software developed by Brigham Young University to perform CC-EBSD analysis using real, kinematically simulated or dynamically simulated reference patterns (Brigham Young University, 2015).

2.2.1. Tetragonality. The first approach to resolving pseudosymmetric orientations in γ-TiAl employed *OpenXY* to calculate the absolute strain of the patterns using dynamically simulated reference patterns. The absolute strain and orientation were calculated with a previously reported iterative methodology (Fullwood *et al.*, 2015; Kacher *et al.*, 2009; Jackson *et al.*, 2016). As mentioned in the *Introduction*, the CC-EBSD technique converts shifts between the patterns themselves into the overall deformation required to transform one lattice state to the other. When comparing two pseudosymmetric orientations, the cross-correlation algorithm will interpret the misaligned *c* axis as a 'pseudostrain' that represents the relative deformation of one pattern with respect to another. The identification of this 'pseudostrain' does not necessarily imply that the lattice itself is in a strained configuration. However, these 'pseudostrains' can be used to detect the pseudosymmetric orientation for which the deformation between the lattices is minimal. Measuring the tetragonality of the cross-correlation for each pseudosymmetric orientation is a simple way of reducing the nine-term strain tensor to a single number that can easily be compared.

The first step was to generate a dynamically simulated reference pattern for the orientation given by the indexing software, which was then used to cross-correlate with the

experimental pattern using a converging iterative algorithm that generates a new reference pattern based on the previous cross-correlation. The deformation gradient tensor provided by the cross-correlation algorithm gave an improved estimate of the relative orientation between the two patterns, which was used to generate the reference patterns for the two additional pseudosymmetric orientations by rotating the lattice by 90° about the *a* axis and 90° about the *b* axis. These patterns were then cross-correlated (without using the iterative algorithm) with the original pattern to determine the deformation gradient tensor between the original pattern and all three of the pseudosymmetric orientations. The tetragonality was calculated for each of the three orientations according to the formula for tetragonality, which is the same calculation as equation (1) when converted to strain:

$$\varepsilon^{\text{tet}} = \varepsilon_{33}^{\text{crystal}} - (\varepsilon_{11}^{\text{crystal}} + \varepsilon_{22}^{\text{crystal}})/2. \quad (2)$$

When the *c* axes of the reference and original lattice are aligned, the lattices will be nearly identical so that all relative strain components should be approximately zero. When the *c* axes are not aligned, the ε_{33} term will decrease, and either ε_{11} or ε_{22} will increase, resulting in a negative tetragonality. Therefore, nonnegative tetragonality should indicate the correct orientation for the original lattice. In the case where the patterns did not align well and there was more than one nonnegative tetragonality, the orientation with the largest positive tetragonality was selected. The method used tetragonal instead of cubic reference patterns in order to more closely approximate the expected lattice geometry. Jackson *et al.* (2016) demonstrated that the best results are obtained when using dynamical reference patterns with less than a 2% relative tetragonality with the experimental patterns. Since γ-TiAl's 2% tetragonality is on the edge of this limit, tetragonal reference patterns were used to achieve the best possible cross-correlation.

In addition to tetragonality, other methods were used in an attempt to match the original pattern with the correct pseudosymmetric reference pattern. We used the same three pseudosymmetric, dynamically simulated reference patterns generated by *OpenXY* and *EMsoft*, and several parameters that quantify the correlation between the original pattern and each reference pattern were recorded. These include the cross-correlation coefficient, mutual information, shift confidence and sum of squared error.

2.2.2. Cross-correlation coefficient. The normalized cross-correlation coefficient *r* is a pixel-by-pixel comparison between two patterns, defined as (Winkelmann *et al.*, 2014)

$$r = \frac{1}{n}\sum_{x,y}\frac{[f(x,y)-\bar{f}][t(x,y)-\bar{t}]}{\sigma_f\sigma_t}, \quad (3)$$

where *f* and *t* are the grayscale values of the two patterns, $\bar{f}$ and $\bar{t}$ are the average grayscale pixel values aross the image, σ_f and σ_t are the standard deviations of the images, and *n* is the number of points in the images. The coefficient will approach 1 for identical images and 0 for images with zero correlation. In EBSD, it has been used to qualitatively compare the fidelity of simulated patterns by evaluating how closely they replicate an experimental image (Winkelmann *et al.*, 2014).

2.2.3. Mutual information. Mutual information is another method for performing image comparison that has been introduced into the materials science community in recent years (Gulsoy *et al.*, 2009). This parameter is reported to be a more robust method of comparing two images than conventional cross-correlation techniques, so will also be used to attempt to resolve pseudosymmetry. The mutual information is calculated by computing the entropies of the two individual patterns as well as the joint entropy. The individual entropy is calculated by first computing the normalized histogram $p_i = h(i)/N$ of the image, where $h(i)$ is the histogram of the image for gray levels between 0 and 255, and *N* is the number of pixels in the image. The entropy is then defined as $H(A) \equiv -\sum_{i=0}^{255} p_i \ln p_i$. The joint entropy is calculated in a similar manner by first computing the joint histogram $h(i, j)$ of the two patterns, which, when normalized, estimates the probability $p_{ij} \equiv h(i, j)/N$, where *N* is the number of pixels in the pattern. The entropy is then calculated as $H(A, B) = -\sum_{i,j}^{255} p_{ij} \ln p_{ij}$. The mutual information of images *A* and *B*, $I(A, B)$, is then defined as follows (Gulsoy *et al.*, 2009):

$$I(A, B) \equiv H(A) + H(B) - H(A, B). \quad (4)$$

2.2.4. Shift confidence. Another potential method of quantifying the quality of the fit between two images is by comparing the sharpness of the peak of the convolution used during the cross-correlation. The convolution of two images results in a peak at the pixel location corresponding to the shift required to align the two images. For similar images, as is typically the case, the convolution is a 'hump' with a discrete height and width. Therefore the magnitude of the peak of the convolution in terms of standard deviations of the entire convolution can be used as an additional measurement of image similarity. For the current study, the shift confidence between two images, $C(A, B)$, is defined as follows for a convolution of images *A* and *B*, $R(A, B)$:

$$C(A, B) \equiv \frac{\max[R(A, B)] - \bar{R}(A, B)}{\sigma_{R(A,B)}}. \quad (5)$$

The cross-correlation algorithm selects many sub-regions of the patterns to compare using convolutions. These sub-regions are commonly referred to as regions of interest or ROIs. The combined shift of each of these regions is used to calculate the shift of the entire pattern (Kacher *et al.*, 2009; Fullwood *et al.*, 2015; Jackson *et al.*, 2016). The shift confidence is also calculated for each of these regions, and the average over all of the regions was used to compare each pseudosymmetric orientation. The current study used 48 ROIs arranged in a grid pattern as described by Jackson *et al.* (2016).

2.2.5. SSE. The last value used to attempt to quantify the similarity between two images is referred to as the SSE, or sum of squared error, of the cross-correlation. This is calculated as the sum of squares of the lengths of the shifts for each of the ROIs. The SSE of the cross-correlation is simply the norm of

the deformation tensor between the two images, which is proportional to the shift required to align the regions of interest; therefore, the more similar the images are, the smaller the shift required to align them and the smaller the value of the SSE.

2.2.6. Hybrid. It is possible that no single one of the previously described methods provides better results in all situations. In cases where relative merits of particular methods can be identified, a combination of several of the methods, or a hybrid method, may prove to be advantageous in order to combine strengths of different methods to produce a better overall result.

2.3. Pattern center calibration

The pattern (or projection) center (PC) calibration is critical for accurate and precise determination of lattice orientation from EBSD and subsequent CC-EBSD analysis. The EBSD system can be calibrated using a variety of methods, including a known single crystal (Dingley & Baba-Kishi, 1986), shadow-casting (Biggin & Dingley, 1977; Venables & Bin-Jaya, 1977; Mingard *et al.*, 2011) or camera calibration (Wright, 1992; Hjelen *et al.*, 1993; Maurice *et al.*, 2011). In practice, the PC is most often determined using an iterative procedure first proposed by Krieger Lassen (1999); the popularity of this method is due to its balance of convenience and accuracy.

The PC calibration is performed by first detecting the bands in the pattern by either using the Hough transform or manually locating the bands. The second step is to make an initial estimate of the calibration values (hereafter x^*, y^* and z^*, where x^* and y^* are the coordinates of the PC in the phosphor screen of the detector and z^* is the sample-to-screen distance). When the pattern is indexed using this initial estimate, the bands in the overlay solution should be sufficiently close to those in the experimental pattern that the indexing solution is able to provide a good enough estimate to start the process. The x^*, y^* and z^* values are then varied, the pattern re-indexed using the same band positions, and the orientation redetermined. From the new orientation, the average angular fit (Nowell & Wright, 2004) between the indexing solution and the detected bands is determined. The fit is the parameter used to judge whether the new pattern center is better than the previous estimate. In the *OIM* software used in the current study (EDAX, 2015) this procedure is termed 'PC tuning'.

The *OIM* software varies x^*, y^* and z^* by a value $\pm 1\%$ from the starting position (x_0^*, y_0^*, z_0^*). (1% meaning 1% of the camera diameter in pixels.) The pattern is indexed using a PC at each of the following eight coordinates:

$$(x_0^* - 1\%, y_0^* - 1\%, z_0^* - 1\%),$$

$$(x_0^* + 1\%, y_0^* + 1\%, z_0^* + 1\%),$$

$$(x_0^* + 1\%, y_0^* - 1\%, z_0^* - 1\%),$$

$$(x_0^* - 1\%, y_0^* + 1\%, z_0^* + 1\%),$$

$$(x_0^* - 1\%, y_0^* + 1\%, z_0^* - 1\%),$$

$$(x_0^* + 1\%, y_0^* - 1\%, z_0^* + 1\%),$$

$$(x_0^* - 1\%, y_0^* - 1\%, z_0^* + 1\%),$$

$$(x_0^* + 1\%, y_0^* + 1\%, z_0^* - 1\%),$$

which are essentially a set of vertices defining a box in PC space centered at the starting PC position. After indexing, the fit at each position is determined and the position producing the minimum fit identified. If the minimum fit at one of these points is less than that obtained at the starting position, then the procedure is repeated until the fit at the starting position is less than that of all the points at the corners of the surrounding box. The same procedure is repeated for a step size of 0.1% and again at 0.01%. For a 480 × 480 pixel pattern this is equivalent to about 0.05 pixels. However, this is not to claim that the accuracy of the PC method is less than a tenth of a pixel – this is simply the output of the algorithm. A recent study has shown that this approach gives good results for general orientation determination (Ram *et al.*, 2015), but other work has shown that CC-EBSD measurements generally require more accurate determination of the PC (Britton *et al.*, 2010).

In the case of γ-TiAl and pseudosymmetry, this procedure needs to be performed three times with the starting orientation set to each of the three pseudosymmetric solutions. In addition, the procedure is modified slightly so that during the iterative process of stepping through the different PC positions the orientations obtained after re-indexing remain near the original starting orientation, to ensure that the algorithm is not switching from one pseudosymmetric orientation to another. After the PC tuning is performed for all three pseudosymmetric candidate orientations, the candidate producing the minimum fit value is assumed to be the correct solution (Zambaldi *et al.*, 2009) and that producing the best estimate of the PC.

2.4. Pattern center sensitivity

Pattern center error results in small relative shifts between the experimental pattern and the simulated reference pattern, introducing artificial strain and orientation error after cross-correlation. Since pseudosymmetric patterns are very similar, it is expected that pattern center error will have a significant effect on the ability to resolve the correct orientation.

In order to determine the pattern center sensitivity of the five potential methods for resolving pseudosymmetry described in the previous section, the same simulated scan of γ-TiAl described in §2.1.1 was used. Since the scan was simulated, the pattern center and orientation of each point were precisely known. The goal was to determine the maximum pattern center error that could be tolerated before the pseudosymmetric orientation was incorrectly identified. This was achieved by incrementally changing the expected pattern center of the 'experimental' pattern relative to the actual pattern center used to generate the dynamically

simulated pattern, thereby simulating increasing pattern center error. The five methodologies described in §2.2 were used to identify which of the three possible pseudosymmetric orientations most closely matched the experimental pattern. The result was then compared with the actual orientation used to generate the pattern and the number of incorrectly resolved points (out of the 100 points in the scan) was recorded.

2.5. Pattern quality sensitivity

Given the similarity of the patterns for pseudosymmetric orientations, it is expected that the quality of the EBSP will affect the ability of the cross-correlation and related image comparison methodologies described in §2.2 to identify the correct orientation. A similar method to the one described in the previous section for determining pattern center error sensitivity was used to determine the sensitivity to pattern quality. Two metrics were used to quantify pattern quality: image resolution and Poisson noise.

The resolution of the images was incrementally reduced by simply binning the original patterns (1024 × 1024 resolution) as they were read into the algorithm. Poisson noise was introduced into the experimental patterns as they were read into the algorithm using the method reported by Hansen *et al.* (2017). The noise and resolution were varied independently. The number of incorrectly resolved pseudosymmetries was identified for each level of binning and noise.

3. Results and discussion

3.1. Simulated scan

Pseudosymmetry in the simulated scan of γ-TiAl was successfully resolved using all six of the methodologies detailed in §2.2. Fig. 2 shows the inverse pole figure (IPF) maps indicating the orientations of the simulated scan; the IPF color mapping is shown in Fig. 3. Fig. 4 shows the misorientation of

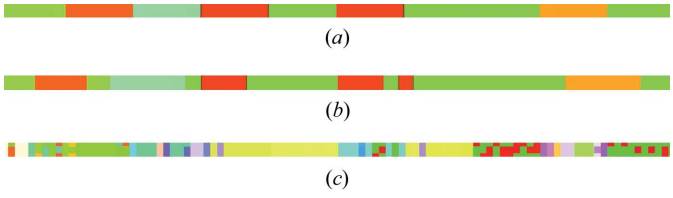

Figure 2
IPF maps of the simulated scans for the actual orientations of the simulated scan (*a*), orientations after indexing with *OIM* (*b*), and orientations after indexing with *OIM* and a resolution reduction of 0.08 (*c*).

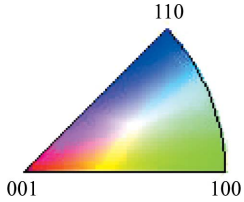

Figure 3
Legend for IPF maps generated by *OIM*, for the [001] direction.

Table 2
Pattern center sensitivities for the five methods.

Pattern center sensitivity is defined as the maximum pattern center error allowed before the method incorrectly identifies the true pseudosymmetric orientation. See caption for Fig. 6 for definition of abbreviations

	Pattern center sensitivity (in percent pattern width)		
Method	**X**	**Y**	**Z**
Tetragonality	0.6	4.0	0.06
Cross-correlation	0.6	0.4	0.8
Mutual information	0.8	0.4	0.8
Shift confidence	2.0	2.0	1.0
SSE	2.0	6.0	0.6

the simulated scan relative to the correct orientations; the misorientation color mapping is shown in Fig. 5. Misorientations of approximately 90° indicate the selection of an incorrect psuedosymmetric orientation.

Ninety percent of the simulated patterns were correctly indexed using *OIM*, as shown in Figs. 2(*b*) and 4(*a*). Each point of the scan was then analyzed with each of the six methodologies. Each methodology was 100% successful in identifying the correct orientation. Since all of the methodologies successfully resolved the pseudosymmetry where traditional Hough-based methods failed, and since the simulated patterns are ideal 'perfect' patterns with excellent image quality and zero pattern-center error, further tests were performed to determine the relative advantages of each of the six methodologies by distorting simulated patterns.

3.1.1. Pattern center sensitivity. Fig. 6 shows the sensitivity of the six methodologies to pattern center error. The sensitivity here is defined as the maximum error allowed before the method begins to mis-index the patterns. The results are also summarized in Table 2. The results were significantly different depending on the direction and the method. In general (with one exception), the pattern error should be kept lower than 0.4% of the pattern width in any direction. For the simulated patterns used in the study, this corresponds to about 4 pixels or 90 µm. The **Z** direction was generally the most sensitive, and the smallest pattern center error that caused an incorrect pseudosymmetry to be selected was 0.06%, corresponding to an allowable error of 0.6 pixels or 13 µm. Previous studies

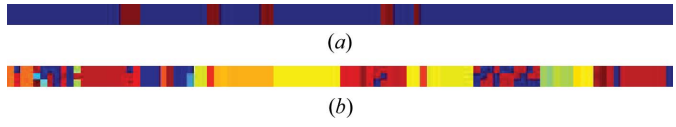

Figure 4
Misorientation maps relative to the correct orientations after indexing with *OIM* (*a*) and after indexing with *OIM* with a resolution reduction of 0.08 (*b*).

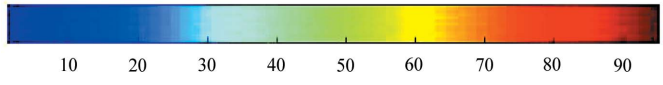

Figure 5
Color bar for misorientation maps.

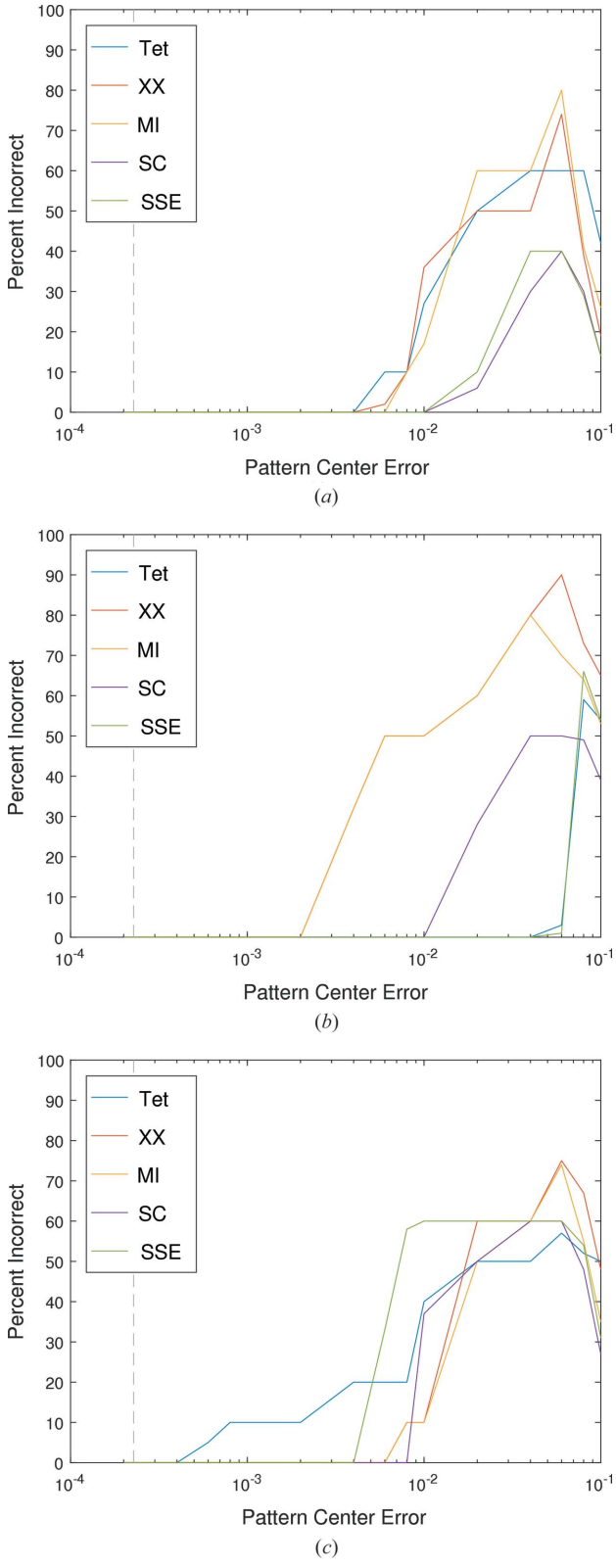

Figure 6
Pattern center sensitivity for the six methods for the **X** direction (*a*), **Y** direction (*b*) and **Z** direction (*c*). Shows the percentage of patterns that are mis-indexed owing to increasing pattern center error. The gray vertical bar shows the typical resolution of pattern center calibration techniques. Abbreviations in the legend are as follows: Tet = tetragonality, XX = cross-correlation coefficient, MI = mutual information, SC = shift confidence.

have shown that current pattern center calibration methodologies can potentially correct the pattern center to within 0.01% of the pattern width (about 4 μm, or about one-fifth of a pixel) (Jackson *et al.*, 2016; Basinger *et al.*, 2011) and can therefore reduce the pattern center error to values within the sensitivity of any of the methodologies. The results for the current experiment matched the expected tetragonal behavior of pseudosymmetric grains, also indicating that the pattern center measurement is adequate.

Fig. 7 shows the results of reducing the resolution of the pattern using standard binning techniques. These results show that most of the techniques are fairly robust to low resolutions: most of the techniques were able to successfully resolve images with a resolution as low as 82 × 82 pixels (Fig. 8). At the same resolution, Hough-based indexing selected a pseudosymmetry for 36% of the patterns and accurately

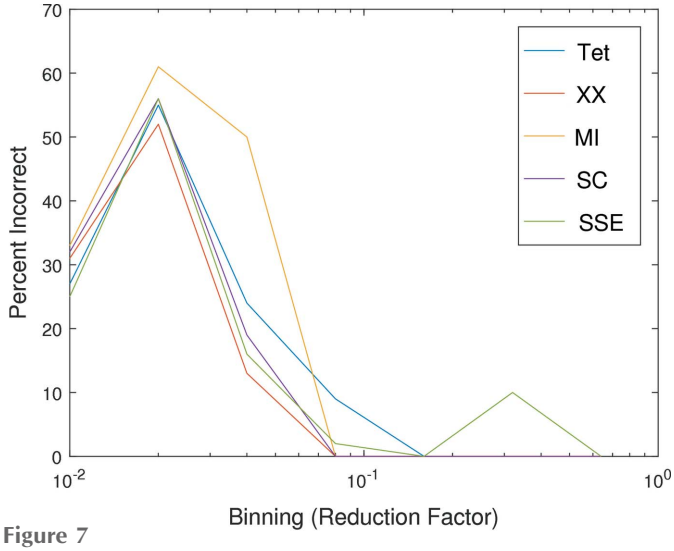

Figure 7
Sensitivity of the six methodologies to pattern resolution. Shows that most methodologies fail at a reduction factor of 0.08, which corresponds to a resolution of about 82 × 82 pixels, like that shown in Fig. 8. See caption for Fig. 6 for definition of abbreviations.

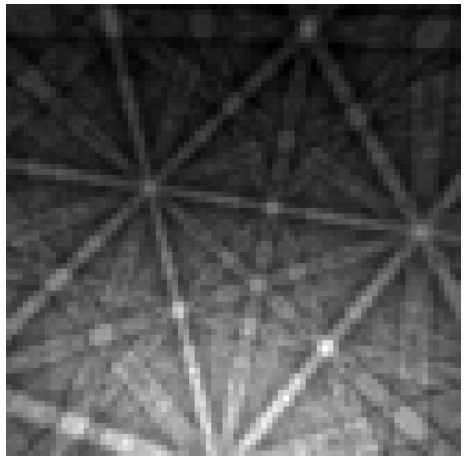

Figure 8
Lowest-resolution pattern whose pseudosymmetry could successfully be resolved.

determined the orientation within 5° for 16% of the patterns (see Figs. 2*c* and 4*b*). The results also show that using tetragonality is slightly more sensitive to resolution than other techniques (with the exception of SSE). This could result from the dependence of the technique on sub-sections of the image, whereas mutual information and cross-correlation coefficients are holistic pattern comparisons and therefore use a larger percentage of the pixels. As the resolution reduces to about 20 × 20 pixels all methods fail between 50 and 60% of the time, which aligns fairly well with the expected purely random selection probability of 66%. Interestingly, as the resolution decreases to 10 × 10, the number of mis-indexed patterns for all methods decreases to about 30%.

3.1.2. Sensitivity to pattern noise. Fig. 9 shows the results of introducing Poisson noise into the simulated pattern using the *poissrnd* MATLAB function (https://uk.mathworks.com/help/stats/poissrnd.html). All methods except using the SSE were able to resolve the pseudosymmetry up to significant levels of noise (see Fig. 10). At the level of Poisson noise shown in Fig. 10, Hough-based indexing could not detect the bands and failed to index the patterns. This demonstrates that CC-EBSD techniques in general are robust to poor pattern quality. An ability to accommodate higher levels of noise allows for higher camera gains, which allows for increased scan speed, reducing drift problems and cost.

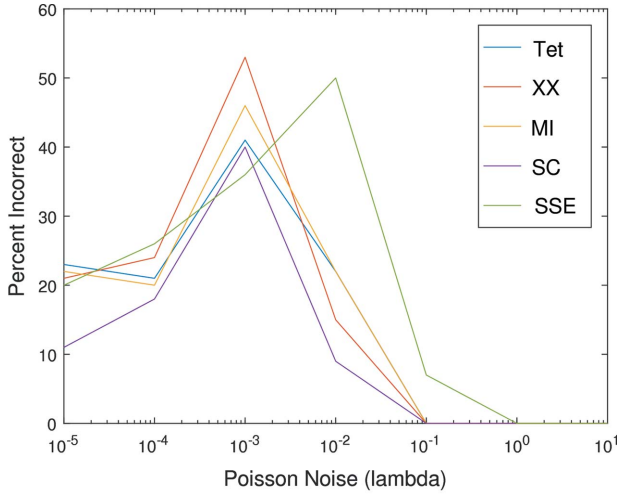

Figure 9
Sensitivity of the six methodologies to pattern noise. Shows that most methodologies fail when the noise increases above that shown in Fig. 10. See caption for Fig. 6 for definition of abbreviations.

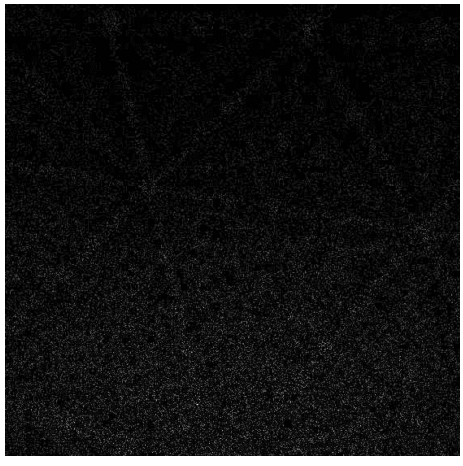

Figure 10
Maximum amount of Poisson noise before pseudosymmetry could not be resolved. The brightness and contrast have been increased for the pattern in order to make the noise of the pattern more easily discernible in this image.

Table 3
Percent pseudosymmetric misorientations.

Percent of points with a local misorientation (in degrees) with their neighbor in the −**Y** scan direction where the misorientation is less than 5°, between 5 and 85°, and greater than 85°. Misorientations of less than 5° correspond to well indexed points in the same grain, whereas misorientations between 5 and 85° correspond to grain boundaries or noise, and misorientations greater than 85° correspond to points that are pseudosymmetric to each other. Therefore, methods with a low percentage of points in the >85° window are desirable. The 'With filter' columns report the same statistic after scan points of low image quality have been removed.

	No filter			With filter		
Method	<5°		>85°	<5°		>85°
Original	83.6%	11.9%	4.5%	93.9%	1.7%	4.4%
Tetragonality	68.9%	23.7%	7.4%	93.7%	3.2%	3.1%
Cross-correlation	67.9%	21.3%	10.8%	93.3%	2.7%	3.9%
Mutual information	68.1%	20.9%	11.0%	93.7%	2.6%	3.7%
Shift confidence	68.3%	23.8%	7.9%	94.8%	3.0%	2.2%
SSE	36.3%	22.5%	41.1%	50.6%	3.1%	46.5%
Hybrid	68.6%	20.6%	10.8%	94.2%	2.6%	3.3%

Interestingly, for all three of the sensitivities evaluated in the current study (PC error, pattern resolution and pattern noise) the effects showed a peak rather than a continually increasing or plateauing behavior. This could be due to artifacts within the CC-EBSD algorithm, where the patterns are so dissimilar that no reliable shifts are determined and the algorithm is biased towards one particular solution, most likely the original solution.

3.2. Experimental scan

In order to differentiate between the various methodologies for resolving pseudosymmetry, the methodology was tested on an experimental sample of γ-TiAl (described in §2.1.2). The pattern center was calibrated using the method described in §2.4 and was adjusted across the scan to account for the shift in pattern center with beam position. After pattern center calibration, each point in the scan was analyzed according to the methodology described in §2.2. Since the analysis evaluated all five methodologies for each point and was not optimized for computational efficiency, the analysis took about 5 s per pattern on a Mac Mini with a 2.6 GHz Intel Core i5 processor.

Fig. 11 shows the IPF maps of the results for each of the five methods (the IPF color mapping for this figure was changed for better visualization and is given in Fig. 12). Fig. 13 shows the misorientation of each point with its neighbor in the negative −**Y** direction (color mapping is given by Fig. 5). Misorientations of about 90° (points shown in red in Fig. 13) are likely to be points that are incorrectly resolved pseudosymmetric orientations, since each of the three

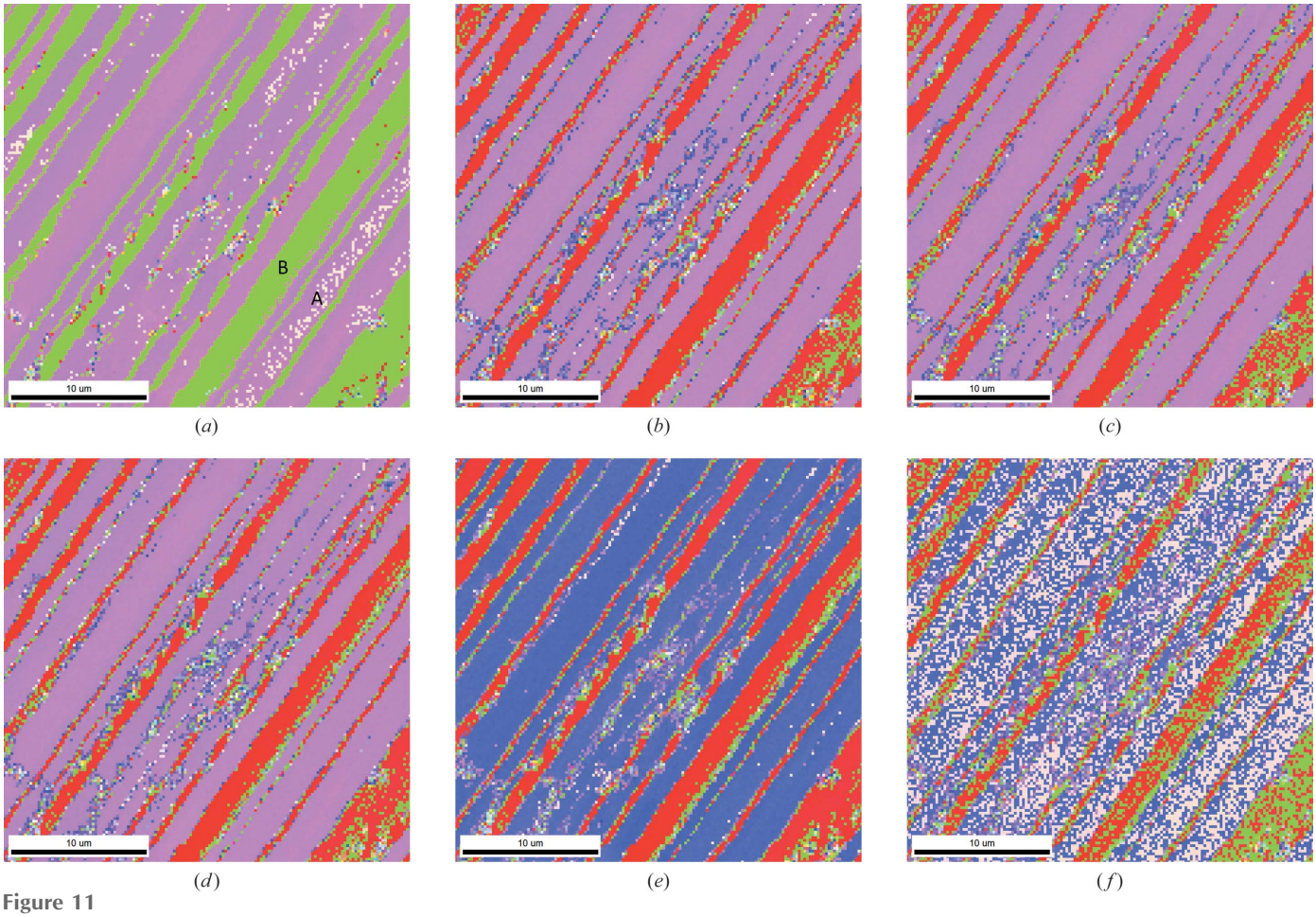

Figure 11
IPF maps of the experimental scan for original *OIM* orientations (*a*), and when the pseudosymmetry was resolved using tetragonality (*b*), the normalized cross-correlation coefficient (*c*), mutual information (*d*), shift confidence (*e*) and SSE (*f*). The IPF color mapping was changed for better visualization and is given in Fig. 12.

pseudosymmetric orientations has a relative misorientation of 90°. Table 3 quantifies the potential accuracy of each method by calculating the percentage of points with misorientations less than 5°, between 5 and 85°, and greater than 85°, corresponding to points within the grain, noise or points at grain boundaries, and points that are pseudosymmetric orientations with their neighbor, respectively. Since the cross-correlation-based methods did not perform well in regions of poor image quality, a filter based upon the Hough-based image quality from *OIM* was used to exclude regions of low image quality (see Fig. 14) and the percentage was recalculated and included in the table. Values below about 75% of the maximum Hough-based image quality were filtered out. Note that the actual number of incorrectly resolved points in the scan will be lower than the percentage given in Table 3, since one isolated incorrectly indexed point will cause two points to have a local misorientation of about 90° (when considering misorientation in a single direction). Therefore, when 3% of the points have a local misorientation greater than 85° this suggests that 3–1.5% of the points were incorrectly indexed. The results show that, when considering all the points in the scan, none of the cross-correlation-based methods chose an orientation as consistently as *OIM*. However, when considering the regions of high image quality, which correspond to the areas of interest for the current study, all of the methods except SSE improved upon the original Hough-based results.

To more directly calculate the number of incorrectly indexed pseudosymmetric points, a baseline orientation has to be selected. There are two predominant orientations in the lamellar structure. These will be denoted as 'A' and 'B', which correspond to the pink and green lamellae in the original IPF map, respectively [see labels in Fig. 11(*a*)]. For each lamella 'family', the orientation that was selected for more than half of the points was selected as the actual orientation for the lamella. The percentage of points in each lamella family that had a misorientation less than 85° with respect to the most

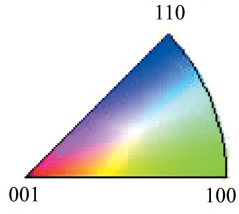

Figure 12
Legend for IPF maps generated by *OIM*, for the [011] direction.

Table 4
Percent pseudosymmetric misorientations by lamella family.

Percent of points with a local misorientation of less than 85° with their neighbor in the −**Y** scan direction by lamella family. The 'With filter' columns report the same statistic after scan points of low image quality have been removed. The lamella family designation is shown in Fig. 11(*a*).

	No filter		With filter	
Method	A bands	B bands	A bands	B bands
Original	96.9%	99.1%	96.1%	99.9%
Tetragonality	98.8%	87.2%	99.8%	90.8%
Cross-correlation	98.4%	84.2%	99.8%	89.2%
Mutual information	97.5%	90.5%	99.2%	94.5%
Shift confidence	96.0%	93.6%	99.2%	98.0%
SSE	59.6%	75.2%	57.3%	72.6%
Hybrid	98.2%	90.5%	99.7%	94.5%

common orientation is recorded in Table 4. The two lamella families were identified by selecting a point in each family and then finding all the points in the scan that had a misorientation of less than 5° with respect to that point, using a set of cubic instead of tetragonal symmetry operators. The 'A' bands appear to have the most pseudosymmetry problems in the original IPF map [the off-white color shown in Fig. 11(*a*)].

3.2.1. Tetragonality, cross-correlation coefficient and mutual information. As shown in Figs. 11 and 13, the original map as indexed by *OIM* (Fig. 11*a*) is very clean but lacks some of the clarity, especially for the thinner lamellae, shown in maps corresponding to the tetragonality, cross-correlation coefficient and mutual information approaches (Figs. 11*b*, 11*c* and 11*d*). Additionally, there are several lamellae with 'noisy' orientations that indicate that the Hough-based indexing is switching between pseudosymmetric orientations [see the lamella with the label 'A' in Fig. 11(*a*)]. Tetragonality, the cross-correlation coefficient and mutual information all performed exceptionally well in resolving the pseudosymmetry in the scan, and resolved about 99% of the points of high image quality in the 'noisy' 'A' lamellae, whereas the traditional Hough-based indexing selected a consistent pseudosymmetric orientation for about 96% (see Table 4). But, these methods did worse than the Hough-based methods in the 'B' lamellae (89–95% for the cross-correlation methods *versus* 99.9% for the *OIM* results).

However, the cross-correlation-based methods selected a different pseudosymmetric orientation for the 'B' bands. The tetragonality matched the predicted behavior fairly well, where the true orientation has near-zero or positive

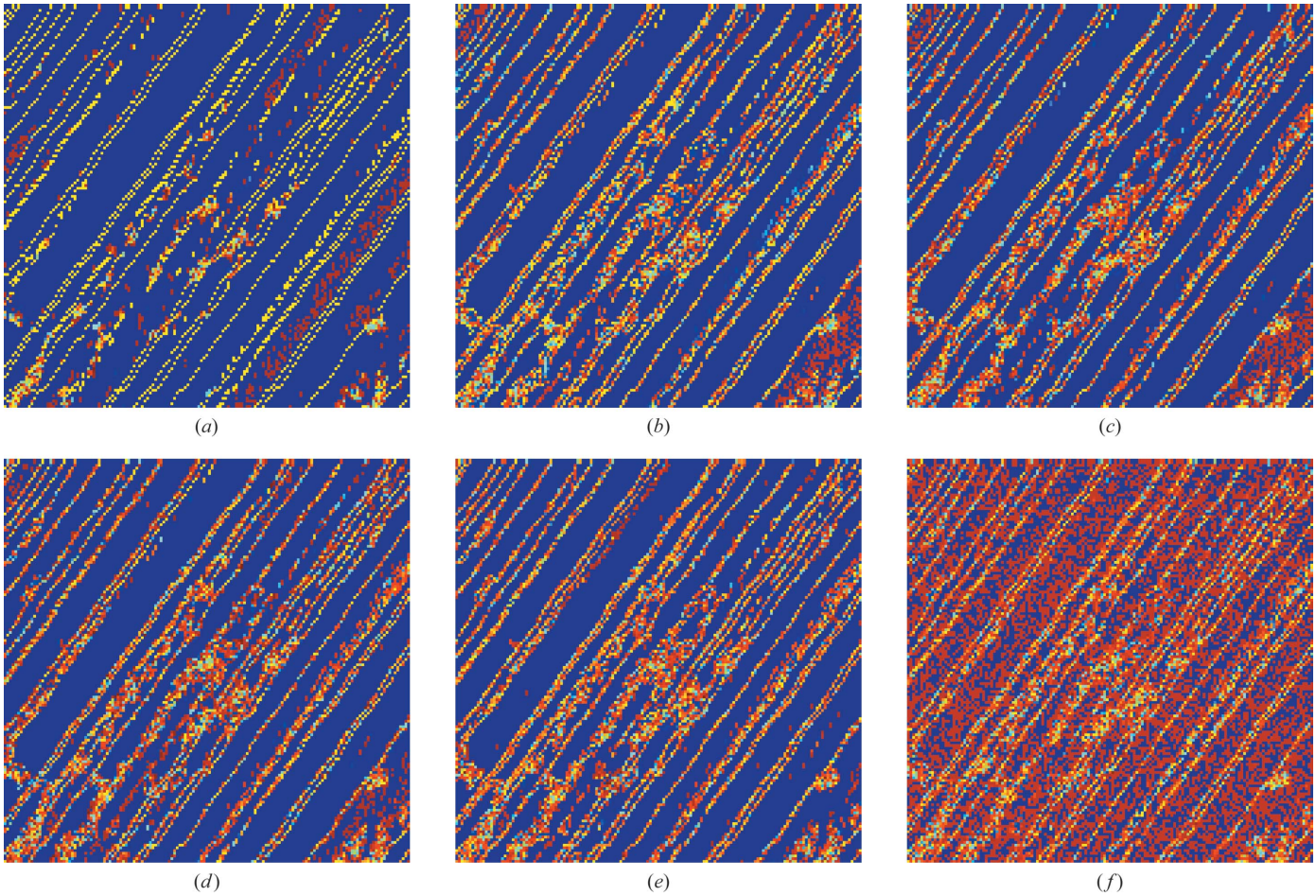

Figure 13
Misorientation maps of the experimental scan for original *OIM* orientations (*a*), and when the pseudosymmetry was resolved using tetragonality (*b*), the normalized cross-correlation coefficient (*c*), mutual information (*d*), shift confidence (*e*) and SSE (*f*).

Table 5
Percentage of points correctly indexed.

Percent of points that were correctly indexed, on the basis of the orientations determined with the detection of the *c* axis using cross-correlation (*i.e.* tetragonality), by lamella family. The 'With filter' column reports the same statistic after scan points of low image quality have been removed. The lamella family designation is shown in Fig. 11(*a*).

	No filter			With filter		
Method	Both	A	B	Both	A	B
Original	71.1%	96.9%	0.5%	74.2%	96.1%	0.0%
Tetragonality	95.7%	98.8%	87.2%	97.7%	99.8%	90.8%
Cross-correlation	94.6%	98.4%	84.2%	97.4%	99.8%	89.2%
Mutual information	95.6%	97.5%	90.5%	98.1%	99.2%	94.5%
Shift confidence	27.2%	3.0%	93.6%	22.6%	0.3%	98.0%
SSE	19.9%	5.5%	59.4%	14.9%	1.2%	61.4%
Hybrid	96.1%	98.2%	90.5%	98.5%	99.7%	94.5%

tetragonality with the reference pattern, and the other two have negative tetragonalities of between 2 and 3%, and the cross-correlation coefficient and mutual information both had one value that was higher than two similar or nearly identical values. Assuming that the cross-correlation method successfully identified the elongated *c* axis by calculating the tetragonality and that therefore the orientations identified by tetragonality, the cross-correlation coefficient and mutual information are the correct orientations, the overall accuracy of each method is given in Table 5. Since the behavior of tetragonality, the cross-correlation coefficient and the mutual information all matched that expected for pseudosymmetric patterns and selected the same orientation, identifying that orientation as the correct orientation is a fairly safe assumption. If this is the case, these three cross-correlation-based methods correctly indexed 97–98% of the points of high image quality, compared to 74% for the Hough-based methods.

3.2.2. Shift confidence. Shift confidence also performed well at consistently selecting a particular orientation (as shown by the lack of random points within a grain with 90° misorientations from their neighbor) but chose a different orientation for the 'A' lamellae than tetragonality, the cross-correlation coefficient and mutual information [see the change in the IPF maps in Fig. 11 from green for maps (*a*)–(*d*) to blue in map (*e*)]. This is probably because shift confidence is not a direct measure of correlation, like the cross-correlation coefficient or mutual information, and instead is a measure of how well the convolution can determine a precise shift. It is possible that a combination of pattern center error and poor pattern quality contribute to a case where the shift is better defined for an incorrect pseudosymmetry. However, it is also possible that shift confidence is selecting the correct orientations while tetragonality, the cross-correlation coefficient and mutual information are not; in the previous section it was shown that shift confidence is generally the least sensitive to both pattern center error and image quality. Without using more advanced validation techniques such as analysis with a transmission electron microscope, it remains uncertain as to what the true orientation actually is. However, since tetragonality, the cross-correlation coefficient and mutual information all selected the same orientation and are more holistic and traditional methods of comparing patterns, it is most likely that they represent the true orientation.

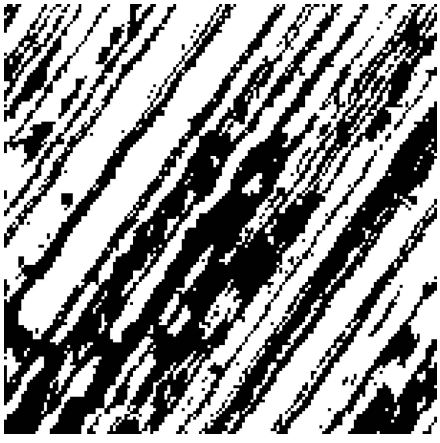

Figure 14
Plot of the filter overlay to exclude regions of low pattern quality. Black areas were excluded and white areas were included.

3.2.3. SSE. The last potential measure of correlation between patterns, SSE, was clearly not effective at differentiating between the pseudosymmetric orientations, as suggested by the very noisy IPF map shown in Fig. 11(*f*).

3.2.4. Hybrid method. Even though tetragonality, the cross-correlation coefficient and mutual information all chose the same orientations, none perfectly resolved the pseudosymmetry in all the lamellae. Of the three methodologies, mutual information performed the best at finding a consistent orientation in the B lamellae, but performed slightly worse in the A lamellae. Therefore a 'hybrid' method that systematically uses either tetragonality or the cross-correlation coefficient in areas of high confidence and mutual information as an alternative could produce better results overall. The confidence of the resolution using the cross-correlation coefficient was quantified as the average separation of the cross-correlation coefficients, denoted $XX_{\rm sep}$, and was calculated as follows:

$$XX_{\rm max} = \max(XX_{1,2,3}), \tag{6}$$

where $XX_{1,2,3}$ is a three-element array of the cross-correlation coefficients of the pattern with each of the three pseudosymmetric reference patterns, and

$$XX_{\rm mins} = (XX_{1,2,3} \neq XX_{\rm max}), \tag{7}$$

where $XX_{\rm mins}$ is a two-element array of the coefficients that are not the maximum. The separation is therefore calculated as

$$XX_{\rm sep} = \left| XX_{\rm max} - \frac{\sum XX_{\rm mins}}{2} \right|. \tag{8}$$

A large value of $XX_{\rm sep}$ would indicate that a pattern was clearly better correlated to the experimental pattern than the other two, whereas a small or near-zero difference would indicate an ambiguous selection between the three patterns. This difference was large in the central region of most of the A lamellae and low at the boundaries, and fairly low in the B lamellae (see Fig. 15). A threshold value of 0.008 was selected,

above which the cross-correlation coefficient would be used to choose the correct pseudosymmetric orientation and below which the mutual information would be used to identify the correct orientation. The result is shown in Figs. 16 and 17. As shown, overall this method cleans up the map better than either method individually. The areas that clearly do not resolve well correspond to areas of poor image quality, as shown in Fig. 16, where the image quality overlays the IPF in grayscale. Fig. 18 shows the misorientation of the results from the hybrid method relative to the original orientations as indexed by *OIM* and shows that most of the B lamellae were rotated by 90°, indicating that *OIM* could have incorrectly indexed the large majority of the patterns in these areas.

In order to assess whether the *OIM* or hybrid results correctly identified the *c*-axis direction of the tetragonal structure, it is noted that the laminar structure in the sample consists of alternating ordered domains. Such domains have specific relationships that have been previously classified (Yamaguchi & Umakoshi, 1990). In the case of the orientations determined by both the *OIM* and the hybrid method, if a cubic structure were assumed, the relationship between neighboring domains would involve a 60° rotation about a ⟨111⟩ axis. However, Yamaguchi & Umakoshi (1990, p. 65) detail only six specific relationships that might exist between {110} directions of the neighboring domains, and related *c*-axis constraints. The *c*-axis constraints are not met by the *OIM* orientations but are met by those determined by the hybrid approach. This analysis verifies that the hybrid results not only provide high precision but also provide correct determination of the *c*-axis directions.

While the precision provided by the hybrid method is high in the A lamellae (as high as 99.8% when using either tetragonality or the cross-correlation coefficient in areas of high image quality), it actually provided lower precision than the results of *OIM* in the B lamellae. It is possible that there is a slight difference in the tetragonality exhibited in these different lamellae, perhaps caused by slightly different Ti to Al ratios. It is also possible that there is an orientational dependency to the hybrid algorithm, such that it performs better at some orientations than others (relating to specific bands and

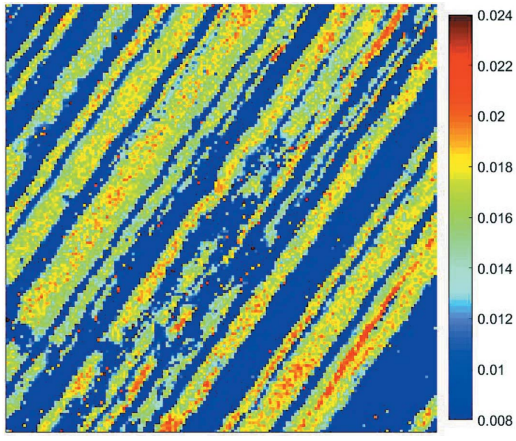

Figure 15
Plot of the separation between cross-correlation coefficients, defined as the average difference of the highest coefficient from the other two coefficients.

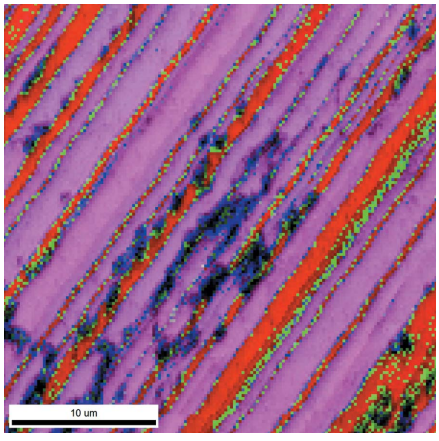

Figure 16
IPF map with grayscale image quality overlay of the scan when resolved using tetragonality. Shows that the poorly indexed regions correspond to regions of poor image quality.

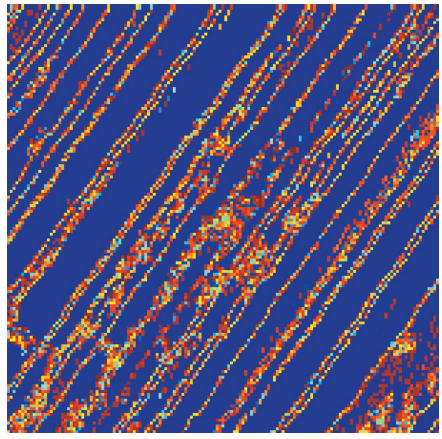

Figure 17
Misorientation map of the scan when resolved using a hybrid method using both tetragonality and the cross-correlation coefficient.

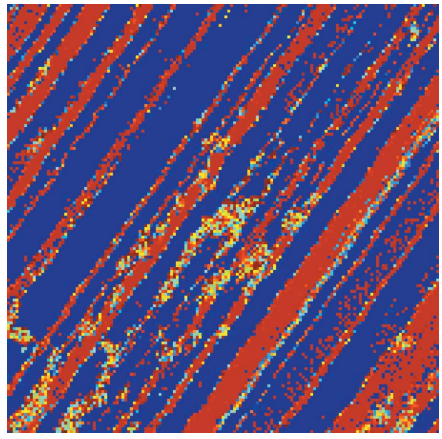

Figure 18
Misorientation map between the points in the scan as resolved by the hybrid method and the original orientations as indexed by *OIM*.

intersections captured in the simulated patterns). However, the cross-correlation methodologies were fairly successful at correcting the *c*-axis predictions given by *OIM*.

Overall, the results show that CC-EBSD can be used to effectively resolve pseudosymmetry in γ-TiAl. The hybrid approach discussed here, which combines the relative merits of the cross-correlation coefficient and the mutual information, yields the best results; however, the shift confidence approach also performed exceptionally well and may benefit from further analysis as a potential metric for measuring the correlation between images. While the methodology performed well in the central regions of most of the bands, locations of poor image quality resulted in lower precision than the Hough-based method, suggesting that the method may be more sensitive to poor pattern quality than implied by the noise analysis performed using simulated patterns; the pattern quality metrics of pattern resolution and Poisson noise used in the current study may not completely capture the actual phenomena of poor pattern quality.

Even though none of the methodologies were 100% successful at resolving the pseudosymmetry in the experimental sample, the hybrid methodology performed better than the Hough-based techniques used previously and cleaned up the orientations of the sample, uncovering microstructural information that was not readily apparent beforehand. This increased microstructural information may aid future research leading to better characterization of γ-TiAl.

4. Conclusion

This paper successfully builds upon other studies, showing that cross-correlation electron backscatter diffraction with dynamically simulated reference patterns can be used to resolve pseudosymmetry in materials with near-unity tetragonality, such as γ-TiAl. By analysis of simulated scans of γ-TiAl, the pseudosymmetry was successfully resolved for 100% of the scan for patterns free of pattern center error and at full resolution (1024 $\times$ 1024 pixels). The theoretical limits of the methodology were established and were found to be fairly robust to pattern center error, pattern resolution and pattern noise, successfully resolving the pseudosymmetry for pattern center errors up to about 13 µm, pattern resolutions of 82 $\times$ 82 pixels and Poisson noise with $\lambda = 0.1$. Subsequent studies could address the use of image processing to potentially mitigate the effects of noise.

The results of the analysis of an experimental sample of γ-TiAl demonstrated the capability of the methods set forth in this study to resolve pseudosymmetry in lamellar γ-TiAl. These methods successfully indexed about 96% of the points in the scan, with correct *c*-axis identification verified using known relationships between neighbors in ordered domains of γ-TiAl. Of the several methodologies evaluated in this study – namely a calculation of tetragonality, the normalized cross-correlation coefficient, mutual information, shift confidence and SSE of the cross-correlation – a hybrid method utilizing both the normalized cross-correlation coefficient and the mutual information successfully resolved areas that Hough-based indexing methods failed to consistently index and revealed microstructure that was not immediately apparent before resolving the pseudosymmetry. The cross-correlation coefficient, the mutual information and a measurement of tetragonality using CC-EBSD analysis all produced very similar results for the given sample. The study also demonstrated a new methodology for performing the pattern center calibration to achieve very good results even with Hough-based indexing. While the Hough-based results for the current sample performed remarkably well at selecting a consistent orientation, the cross-correlation methods suggest that the Hough-based method erroneously indexed one of the two sets of unique orientations within the sample, accounting for nearly 25% of the scan. Therefore, the results for the sample analyzed in the current study suggest that Hough-based methods may consistently select a pseudosymmetric orientation, but cross-correlation methodologies should be used to more confidently identify the correct pseudosymmetric orientation in γ-TiAl.

The study showed that the cross-correlation coefficient and mutual information can be effectively used to consistently identify minute differences between patterns. The use of tetragonality calculations from CC-EBSD to resolve pseudosymmetry also illustrates the potential of CC-EBSD to measure absolute strain and therefore tetragonality. Shift confidence, a measure of the height of the convolution of subregions of the patterns, also performed exceptionally well and had excellent robustness to pattern center error, poor pattern resolution and image noise. However, it chose a different pseudosymmetric orientation when resolving the pseudosymmetry in the experimental scan, compared to the cross-correlation coefficient, mutual information and tetragonality. As a new measure of correlation proposed in this study, it may deserve further consideration and evaluation for its use within the CC-EBSD methodology. The SSE of the cross-correlation coefficient failed to resolve the pseudosymmetry in the experimental scan.

Funding information

The BYU team was supported by US Department of Energy (DOE), Office of Science, Basic Energy Sciences (BES), under award No. DE-SC0012587.

References

Adams, B., Wright, S. & Kunze, K. (1993). *Met. Mater. Trans. A*, **24**, 819–831.
Alkorta, J. (2013). *Ultramicroscopy*, **131**, 33–38.
Basinger, J., Fullwood, D., Kacher, J. & Adams, B. (2011). *Microsc. Microanal.* **17**, 330–340.
Biggin, S. & Dingley, D. J. (1977). *J. Appl. Cryst.* **10**, 376–385.
Brigham Young University (2015). *OpenXY*, https://github.com/BYU-MicrostructureOfMaterials/OpenXY.
Britton, T., Maurice, C., Fortunier, R., Driver, J., Day, A., Meaden, G., Dingley, D., Mingard, K. & Wilkinson, A. (2010). *Ultramicroscopy*, **110**, 1443–1453.
Britton, T. & Wilkinson, A. J. (2012). *Ultramicroscopy*, **114**, 82–95.

Callahan, P. & De Graef, M. (2013). *Microsc. Microanal.* **19**, 1255–1265.
De Graef, M. (2015). *EMsoft 3.0*, http://www.github.com/marcdegraef/EMSoft.
Dey, S., Bouzy, E. & Hazotte, A. (2006). *Intermetallics*, **14**, 444–449.
Dey, S., Morawiec, A., Bouzy, E., Hazotte, A. & Fundenberger, J. (2006). *Mater. Lett.* **60**, 646–650.
Dingley, D. & Baba-Kishi, K. (1986). *Scan. Electron Microsc.* **2**, 383–391.
EDAX (2015). *OIM Data Collection*. EDAX, Draper, UT, USA.
Fullwood, D., Vaudin, M., Daniels, C., Ruggles, T. & Wright, S. I. (2015). *Mater. Charact.* **107**, 270–277.
Gulsoy, E., Simmons, J. & De Graef, M. (2009). *Scr. Mater.* **60**, 381–384.
Hansen, L., Jackson, B., Fullwood, D., Wright, S. I., De Graef, M., Homer, E. & Wagoner, R. (2017). *Microsc. Microanal.* **23**, 460–471.
Hjelen, J., Ørsund, R., Hoel, E., Runde, P., Furu, T. & Nes, E. (1993). *Texture Stress Microstruct.* **20**, 29–40.
Jackson, B., Christensen, J., Singh, S., De Graef, M., Fullwood, D., Homer, E. & Wagoner, R. (2016). *Microsc. Microanal.* **22**, 789–802.
Kacher, J., Basinger, J., Adams, B. L. & Fullwood, D. T. (2010). *Ultramicroscopy*, **110**, 760–762.
Kacher, J., Landon, C., Adams, B. L. & Fullwood, D. (2009). *Ultramicroscopy*, **109**, 1148–1156.
Krieger Lassen, N. (1999). *J. Microsc.* **195**, 204–2011.
Maurice, C., Dzieciol, K. & Fortunier, R. (2011). *Ultramicroscopy*, **111**, 140–148.
Mingard, K., Day, A., Maurice, C. & Quested, P. (2011). *Ultramicroscopy*, **111**, 320–329.
Nolze, G., Winkelmann, A. & Boyle, A. P. (2016). *Ultramicroscopy*, **160**, 146–154.
Nowell, M. & Wright, S. (2004). *J. Microsc.* **213**, 296–305.
Oxford Instruments NanoAnalysis (2016). *EBSD Analysis of TiAl Alloys for Texture and Interphase Boundary Analysis.* Application Note. Oxford Instruments, https://www.oxford-instruments.com/getmedia/c04b55c3-e055-4f61-a4bb-06cc8b119214/EBSD-analysis-of-TiAl-alloys-for-texture-and-interphase-boundary-analysis.
Ram, F., Zaefferer, S., Jäpel, T. & Raabe, D. (2015). *J. Appl. Cryst.* **48**, 797–813.
Sankaran, A., Bouzy, E., Humbert, M. & Hazotte, A. (2009). *Acta Mater.* **57**, 1230–1242.
Schwartz, A. J., Kumar, M., Adams, B. L. & Field, D. P. (2009). *Electron Backscatter Diffraction in Materials Science.* New York: Springer.
Simkin, B., Ng, B., Bieler, T., Crimp, M. & Mason, D. (2003). *Intermetallics*, **11**, 215–223.
Troost, K., Sluis, P. & Gravesteijn, D. (1993). *Appl. Phys. Lett.* **62**, 1110–1112.
Vaudin, M., Osborn, W., Friedman, L., Gorham, J., Vartanian, V. & Cook, R. (2015). *Ultramicroscopy*, **148**, 94–104.
Venables, J. & Bin-Jaya, R. (1977). *Philos. Mag.* **35**, 1317–1332.
Wilkinson, A. J., Meaden, G. & Dingley, D. J. (2006). *Ultramicroscopy*, **106**, 301–313.
Winkelmann, A. (2010). *J. Microsc.* **239**, 32–45.
Winkelmann, A., Nolze, G. & Lühur, T. (2014). EBSD 2014, 17–19 June 2014, Pittsburgh, USA.
Winkelmann, A., Trager-Cowan, C., Sweeney, F., Day, A. P. & Parbrook, P. (2007). *Ultramicroscopy*, **107**, 414–421.
Wright, S. (1992). PhD thesis, Yale University, New Haven, CT, USA.
Wright, S. I., Basinger, J. A. & Nowell, M. M. (2012). *Mater. Sci. Forum*, **702**, 548–553.
Wright, S. I., Nowell, M. M., de Kloe, R. & Chan, L. (2014). *Microsc. Microanal.* **20**, 852–863.
Yamaguchi, M. & Umakoshi, Y. (1990). *Prog. Mater. Sci.* **34**, 1–148.
Zambaldi, C., Zaefferer, S. & Wright, S. I. (2009). *J. Appl. Cryst.* **42**, 1092–1101.